Switching performance of bistable membranes activated with integrated piezoelectric thin film transducers

OPEN ACCESS
IOP Publishing
Journal of Micromechanics and Microengineering
J. Micromech. Microeng. **29** (2019) 105008 (11pp)
https://doi.org/10.1088/1361-6439/ab3185

Switching performance of bistable membranes activated with integrated piezoelectric thin film transducers

M Dorfmeister, B Kössl, M Schneider, G Pfusterschmied and U Schmid

Institute of Sensor and Actuator Systems, TU Wien, 1040 Wien, Austria

E-mail: manuel.dorfmeister@tuwien.ac.at

Received 29 March 2019, revised 1 July 2019
Accepted for publication 11 July 2019
Published 1 August 2019

Abstract

In this paper we report on the fabrication of bistable micro electromechanical systems (MEMS) membranes, which have diameters in the range of 600–800 μm, a total thickness of 3.13 μm and feature integrated low power piezoelectric transducers based on aluminium nitride. To estimate the impact of the membrane asymmetry due to the integrated piezoelectric transducers, an asymmetric constant in the potential energy calculation of the bistable system is introduced, thus enabling a proper theoretical prediction of the membrane behaviour. To switch between the two bistable ground states, rectangular pulses with frequencies in the range of 50–100 kHz and a peak-to-peak voltage of 30 V_{pp} are applied. Two different actuation schemes were investigated, whereas one shows positive and the other negative pulse amplitudes. With a Laser-Doppler Vibrometer the velocity of the membranes during the bistable switching process is measured and integrated over time to calculate the membrane displacement in the centre. FFT (fast Fourier transform) spectra of an applied broadband white noise signal were determined in both ground states and showed a strongly decreased dominant resonance frequency in the lower ground state. The results also showed, that the asymmetry of the system causes different switching behaviours for each bistable ground state, whereas it requires less energy to switch from the lower to the upper ground state. Furthermore, it was demonstrated that a minimum of two pulses are needed for switching when using positive rectangular pulses of 30 V_{pp} in contrast to four when applying negative pulses. The pulse frequency causing switching was in the range of 60–110 kHz, strongly depending on the geometry and applied signal scheme. Additionally, a positive voltage offset applied to the pulse signal characteristics resulted in both a wider range of frequencies suitable for switching and in a decrease of the dominant resonance frequency, which is also beneficial for the switching process and indicates the potential for efficient switching of bistable MEMS membranes.

Keywords: piezoelectric, micro electromechanical systems (MEMS) membranes, aluminium nitride (AlN), bistability

(Some figures may appear in colour only in the online journal)

1. Introduction

In recent years, market segments related to mobile and internet-of-things devices have faced an enormous increase pushing the operation of any component of the system to their specific low power limit to ensure the maximum operation time possible with a given energy source, such as a battery. Given this requirement also the power consumption of micro electromechanical systems (MEMS) sensors and actuators integrated in these systems needs to be reduced to the minimum, as especially nanoelectronics has made remarkable progress to achieve this goal [1–3].

A promising concept for low power MEMS are bistable devices, which have two characteristic stable ground states they can hold without additional energy. This strongly decreases the power consumption when the device is in passive mode. As a consequence, such devices only consume energy when changing between the stable ground states. Furthermore, very high membrane displacements are achievable compared to standard configurations [4]. Common applications for bistable MEMS devices are valves [5–7], relays [8, 9] or energy harvesters [10].

The static bistability of MEMS membranes can be well described with equations based on the standard plate theory [11, 12]. The basic requirement for bistability is the presence of compressive stress in the membrane exceeding the so-called critical stress limit and is usually induced by additional layers on the membrane. If this requirement is fulfilled, the membrane shows buckling behaviour with a characteristic initial displacement. Macroscopic examples for the buckling effect from everyday experience are clicker devices, hair clips and special chassis. To initiate switching between the ground states in MEMS devices, different actuation principles are reported in literature such as electrostatic [8], electromagnetic [5, 9] or thermal transducers [13–15]. In contrast to the latter concepts, it was also reported on using the resonance characteristics of bistable membranes to initiate the switching between the two stable states [16]. To fully exploit all these beneficial properties of bistable membranes device concepts with integrated low-power actuation is needed, as provided by piezoelectric transducers, consisting of a stack of a piezoelectric material sandwiched between a top and bottom electrode. In addition, the piezoelectric layer can also serve as stress inducing layer for the compressive component, thus facilitating device architectures due to a very thin stack and less fabrication steps.

In this study we present bistable membranes with integrated piezoelectric aluminium nitride (AlN) used as both stress inducing layer to achieve bistability and to initiate the switching between the stable ground states by a sequence of voltage pulses. Sputter deposited *c*-axis orientated AlN can be straightforward integrated in a CMOS compatible silicon-based MEMS device process flow and does not require any additional polarisation step. However, to use a piezoelectric material with moderate piezoelectric coefficients [17], special concepts for switching initiation must be applied [18]. In this paper, we introduce two concepts based on rectangular pulses for switching initiation as well as perform an in-depth study on the impact of the pulse frequency. Finally, the different mechanical behaviour of the two ground states will be shown which results in different membrane dynamics depending on the initial ground state prior to switching.

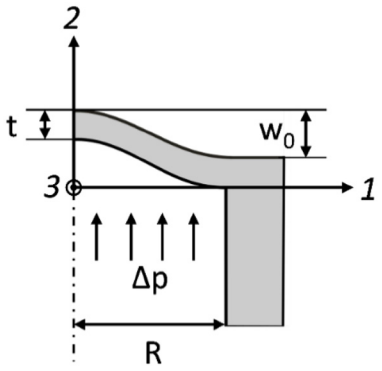

Figure 1. A schematic side view on a bistable membrane indicating the axes and important parameters used in the calculations.

2. Theory

If the intrinsic compressive stress in a membrane exceeds a characteristic value σ_c, the membrane shows bistability. This value strongly depends on the geometry and material parameters of the system. Figure 1 shows the characteristic parameters of a bistable membrane. Under these static conditions, the theoretical description is well known from the membrane theory of Timoschenko [11]. Accordingly, the onset of bistability can also be predicted [7] and is based on the potential energy V in the membrane with consideration of the bending moments:

$$V = \frac{2}{3}\pi w_0 \left(\frac{4}{3} t^3 \frac{E}{1-\nu^2} \frac{w_0}{R^2} + w_0 t\sigma + \frac{16}{35} \frac{E}{1-\nu^2} \frac{t\, w_0^3}{R^2} - \frac{R^2 \Delta p}{2} \right), \tag{1}$$

where E is the Young's modulus, t the thickness, R the radius, ν the Poisson ratio, w_0 the initial buckling height, σ the residual stress in the membrane and the last term represents a asymmetry constant Δp. When the stack would be perfectly symmetric, the asymmetry constant Δp would be zero. As this is not the case for a membrane with stacked layers, this constant is not zero. For membranes consisting of more than one layer, e.g. for electrodes and the piezoelectric layer, the intrinsic layer stress values weighted by the individual thickness are averaged across the membrane thickness [19]. The critical stress can be calculated according to [12] with:

$$\sigma_c = -\frac{4}{3} \frac{t^2}{R^2} \frac{E}{1-\nu^2}. \tag{2}$$

If the stress is higher than this characteristic value, the system has two switchable stable ground states. Rearranging equation (1) while neglecting the asymmetry factor with $\Delta p = 0$ leads to a characteristic quantity related to the potential energy:

$$V \frac{3}{2\pi D} \left(\frac{R}{t}\right)^2 = \left(\frac{w_0}{t}\right)^2 \left(1 - \frac{\sigma}{\sigma_c}\right) + \frac{12}{35} \left(\frac{w_0}{t}\right)^4 \quad \text{with} \quad D = \frac{4}{3} \frac{Et^3}{1-\nu^2}. \tag{3}$$

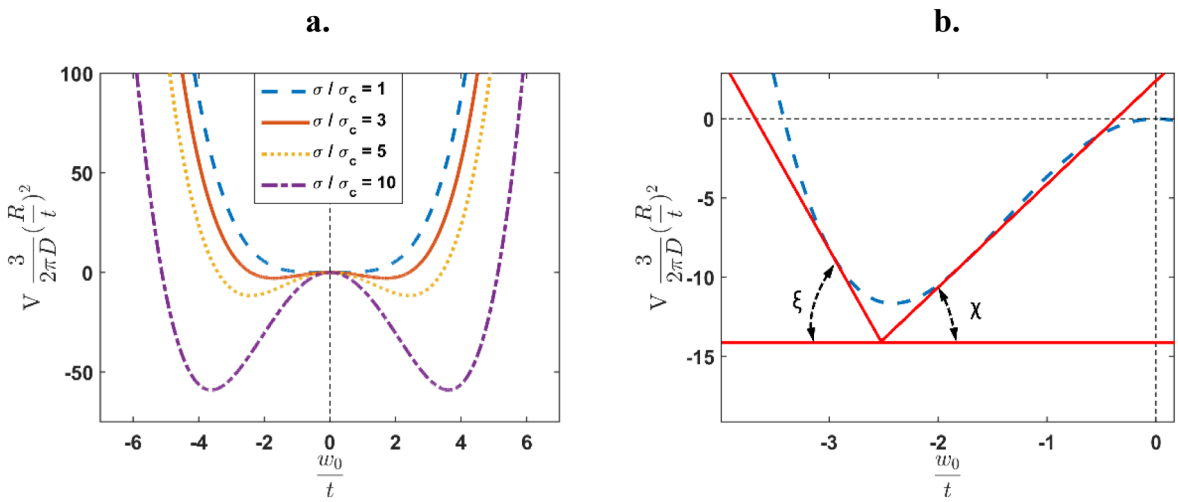

Figure 2. (a) The characteristic quantity (equation (3)) of a bistable membrane ($R = 1$) as a function of the initial deflection and the critical stress as parameter. (b) The characteristic quantity when the stress is constant, but the radius varies resulting in both different critical stress values σ_c and σ/σ_c ratios. (b) The different angles of the potential curves at the turning point close to the left potential energy minimum.

Figure 2 shows the characteristic quantity introduced in equation (3) as a function of the deflection to thickness ratio for different uniform to critical stress σ/σ_c ratios at constant normed radius of $R = 1$. There are two minima for membranes with $\sigma > \sigma_c$ and only one if $\sigma <= \sigma_c$. This demonstrates that for larger ratios σ/σ_c more energy is required to switch between the ground states of the bistable membrane. In addition, the distance between both minima is increased for larger σ/σ_c ratios. Figure 2(b) shows the different slope at the turning point, where ξ is the angle when the deflection is increased and χ the corresponding value when the deflections gets towards zero deflection. This demonstrates that a higher potential energy has to be overcome when the membrane gets more deflected in the buckled state compared to the situation when the membrane deflection is reduced.

To calculate the potential energy for the used bistable membranes, the values from table 1 are used, where E_{eff} and ν_{eff} are the effective Young's modulus and Poisson's ratio, respectively.

When assuming a bistable membrane with homogeneous stress distribution the theoretical results for the potential energy in bistable membranes are shown in figure 3(a). They indicate, that membrane A with the smallest diameter should be switched easier than the others. The same holds for membrane C compared to membrane B. In this work a stack is deposited on top of the membrane, leading to a structural asymmetry. This asymmetric behaviour can be modelled when an asymmetric constant $\Delta p = 200$ Pa is inserted in equation (1) as illustrated in figure 3(b). As a consequence, this constant causes an asymmetry in comparison between the two potential minima and the upper state gets preferred. Each potential curve shows a different slope, whereas membrane C shows the lowest in the upper ground state when introducing the asymmetry constant (see figure 3(b)).

In this work, AlN is used as piezoelectric material which crystallises in a hexagonal wurtzite crystal structure. For the calculations, the elasticity tensor and the piezoelectric coefficients were used as reported in [20] and [17].

Table 1. Characteristic parameters of the bistable membranes investigated within this study.

Name	Diameter [μm]	t_{ges} [μm]	E_{eff} [GPa]	ν_{eff} [−]	σ_{ges} [MPa]	σ_0/σ_c [−]
A	600				−64.9	2.46
B	700	3.13	178.5	0.129	−54	2.78
C	800				−44.7	2.97

As the initial displacement w_0 of MEMS membranes is much lower than the radius, it is assumed that the membrane behaves as being in a standard, flat condition. The stress change in the piezoelectric layer through applying a voltage to the piezoelectric transducer can be calculated with the following equation [21]:

$$\Delta\sigma_{\text{AlN}} = \left(\frac{1}{2}\frac{C_{13}^2}{C_{33}} - C_{11} - C_{12}\right) d_{31} E_3. \tag{4}$$

Here, C_{xy} represents the entries in the elasticity tensor $\mathbf{C}$ in different crystallographic directions, d_{31} the piezoelectric coefficient in lateral direction, E_3 the electrical field strength between the bottom and top electrode and $\Delta\sigma_{\text{AlN}}$ the stress change caused by the electrical field between the electrodes. The AlN layer features an intrinsic stress caused by the deposition process which depends on different parameters of the sputter deposition process [22]. Consequently, the effective stress in the AlN layer can be calculated from the intrinsic stress in the AlN layer after sputter deposition with σ_{0_AlN} and $\Delta\sigma_{\text{AlN}}$ with the applied electrical field E. In this work the coefficients given in table 2 were used.

When a constant electrical bias voltage is applied across the piezoelectric AlN thin film, a change of the effective stress in the AlN layer and thus a modification of the total effective stress in the whole membrane is induced. A positive bias voltage reduces the total compressive effective stress in the membrane and thus reduces the σ/σ_c ratio.

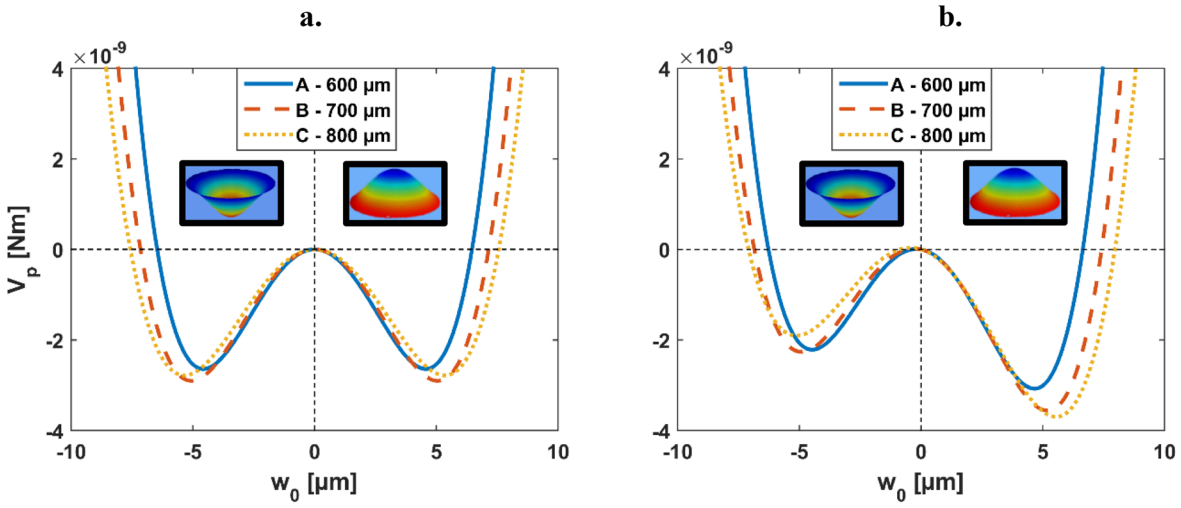

Figure 3. (a) Calculated potential energy characteristics of the membranes investigated in this study without an asymmetry constant $\Delta p = 0$ Pa in equation (1) and (b) with $\Delta p = 200$ Pa (see equation (1)). For illustration purposes pictures of the corresponding bistable ground states are implemented.

Table 2. Mechanical and piezoelectric parameters of AlN.

C_{11} [GPa]	C_{12} [GPa]	C_{13} [GPa]	C_{33} [GPa]	d_{31} [pm V^{-1}]
410 [23]	149 [23]	99 [23]	389 [23]	−1.36 [17]

3. Device fabrication and experimental details

As shown in figure 4 (9), the membrane consists of a stacked structure with a silicon substrate, an insulation layer, a bottom electrode, a piezoelectric AlN layer and a top electrode [24]. The process flow is schematically shown in figure 4. The intrinsic stress in the AlN layer is tailored to achieve bistability. A 100 mm SOI wafer with a device layer thickness of 2 μm, a 1 μm thin buried oxide (BOX) and a double sided protective SiN_x/SiO_2 layer was used as substrate. The SiN_x/SiO_2 layer on the backside was removed with a reactive ion etching process. On the frontside, a 50/200 nm Cr/Au bi-layer was patterned using lift-off to serve as bottom electrode (1 + 2). For the lift-off, an image reversal photoresist AZ5214 from MicroChemicals was used. The same approach was used for structuring the stress tailored AlN layer (3), which was sputter deposited from a 150 mm Al target with a chamber pressure of 2 μbar, a power of 800 W and a nitrogen flow of 50 sccm. These sputter parameters resulted in a compressive stress in the range of 600 ± 50 MPa, measured with the wafer bow method. After the AlN lift-off, the top electrode was structured and deposited in the same way as the bottom electrode (5). Afterwards, the membrane was defined using backside deep reactive ion etching (DRIE), whereas the front side was protected with two layers of AZ6632 photoresist (6). The BOX served as etch stop for the DRIE (7) and was subsequently removed with buffered hydrofluoric acid (HF) (8). Finally, the photoresist was removed and the dies were cut with a wafer saw (9). The total thickness of the membranes is 3.13 μm, consisting of a 2 μm silicon device layer, an 80/250 nm SiN_x/SiO_2 layer, a bottom electrode (200 nm), a piezoelectric AlN layer (400 nm) and a top electrode (200 nm). For the experiments, membranes with diameters of 600, 700 and 800 μm were investigated. The compressive stress of the AlN is not uniformly distributed across the wafer. The lowest compressive stress values are measured in the centre and the highest in the edge region of the wafer. As Table 1indicates, the total stress of this stack is in the range of 50 ± 10 MPa. A SEM image of a membrane with a diameter of 600 μm is shown in figure 5 on the left side, whereas the right side shows an optical micrograph of the die. Only the membranes having a fully covered electrode configuration were investigated in this work.

To measure the dynamic behaviour during the switching between the stable ground states, an MSA-400 laser doppler vibrometer (LDV) from POLYTEC was used. The signal was created in a Matlab program, which drives a programmable function generator AGILENT 33521A. The output signal of the function generator is amplified using a TREK 2100 HF piezo driver with a fixed gain of 50. The output of the amplifier was connected in parallel to the contact needles and the oscilloscope TEKTRONIX TDS2024C, which was used to record the excitation signal. The top electrode is used for applying the stimulation signal, while the bottom electrode is connected to ground. The velocity modulated voltage output of the MSA-400 was connected to a second oscilloscope channel.

As high velocities are expected the output sensitivity of the MSA was set to 1000 mm/s/V. The limiting factor in accuracy, however, is the 8 bit ADC of the oscilloscope. The minimum voltage change of the signal quantisation was measured when connected to a non-vibrating membrane and integrated over time. This results in an accuracy of ±25 nm, which is regarded to be enough for these experiments as total membrane displacements are in the μm range. The displacement transient of the measured velocity signal was calculated via Matlab by integration over the measurement time. The basic principle of the measurements setup is illustrated in figure 6, where the photographs highlight the setup with a contacted sample. The samples are not bonded in a package, so that both electrodes of each sample are connected with two prober needles.

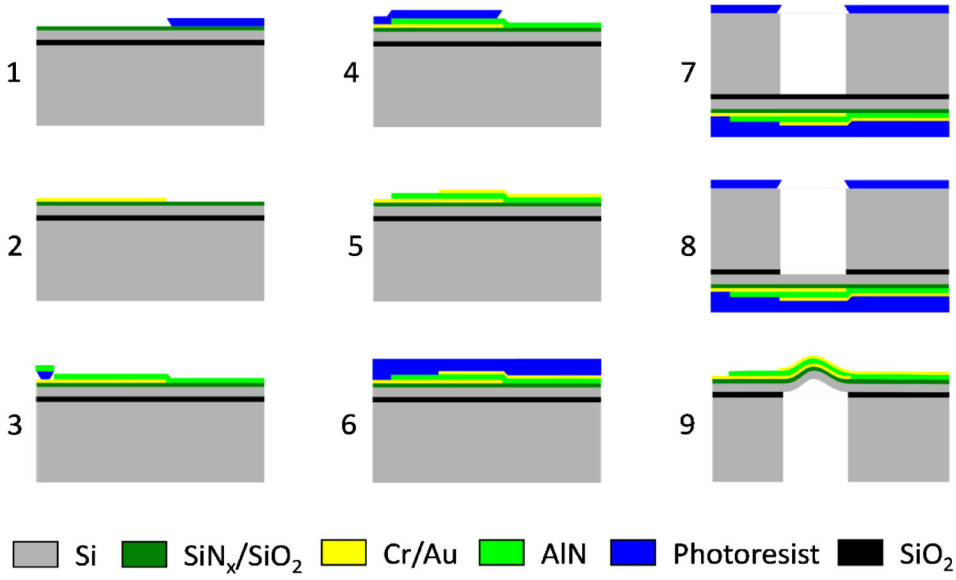

Figure 4. Process flow of the piezoelectric bistable membranes. (1) SOI wafer with SiN_x/SiO_2 layer and structured photoresist (PR) for the lift off of the bottom electrodes, (2) patterned bottom electrodes, (3) structured PR for lift off with sputter deposited AlN, (4) structured PR for top electrode lift off, (5) evaporated and structured electrodes, (6) protective PR for backside DRIE etching (7), the etching of the BOX with HF (8) and the final membrane with released PR (9).

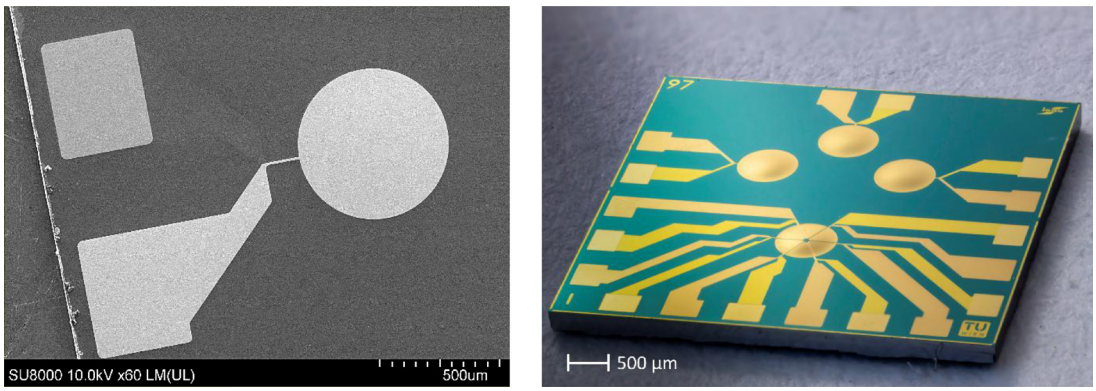

Figure 5. On the left side a SEM picture of a membrane with a diameter of 600 μm is shown, whereas on the right side an optical micrograph of the die is presented.

During the experiments, different rectangular pulse configurations were used, where the frequency was increased stepwise from 50 to 150 kHz by 250 Hz steps. The amount of pulses was fixed to 20 and the duty cycle to 60%. The peak-to-peak voltage was kept constant at 30 V with different offsets in the range of −6 V to 6 V. A bistable switching was detected by the Matlab program when the membrane has experienced a higher displacement than the initial buckling height w_0. An example can be seen in figure 7 where the excitation signal causes a repeated switching between both ground states. The top graph shows the applied signal (blue), the measured velocity (dotted red line) and the bottom graph the calculated displacement transient of a membrane with a diameter of 700 μm. The switching from the upper to the lower ground state is marked with a red arrow and needs three pulses. The aim of the pulses is to swing the membrane to a deflection higher than the zero deflection position. The total displacement of the membrane is measured from the start point to the end point when the membrane has permanently changed the ground state, as shown in figure 7 on the bottom graph.

For the experiments, two actuation schemes were used. In both cases, the bottom electrode was connected to ground, while the top electrode was loaded with the excitation signal. The first scheme (Scheme A) is to apply positive voltage pulses and is also illustrated in figure 8(a), where the top graph shows the applied signal (blue), the measured velocity (red) and the bottom graph the calculated displacement transient. Scheme B uses the same rectangular signal characteristics, but the output of the function generator is inverted. This is shown in figure 8(b). The measurements shown in figure 8 start at the upper ground state, where a positive voltage (Scheme A) results in a displacement to and a negative voltage away from the centre. The same behaviour applies to measurements starting in the lower ground state. When comparing both schemes in figure 8, it can be noticed that the frequency used in scheme A is in good agreement with the bistable switching frequency compared to Scheme B. Only frequencies which are

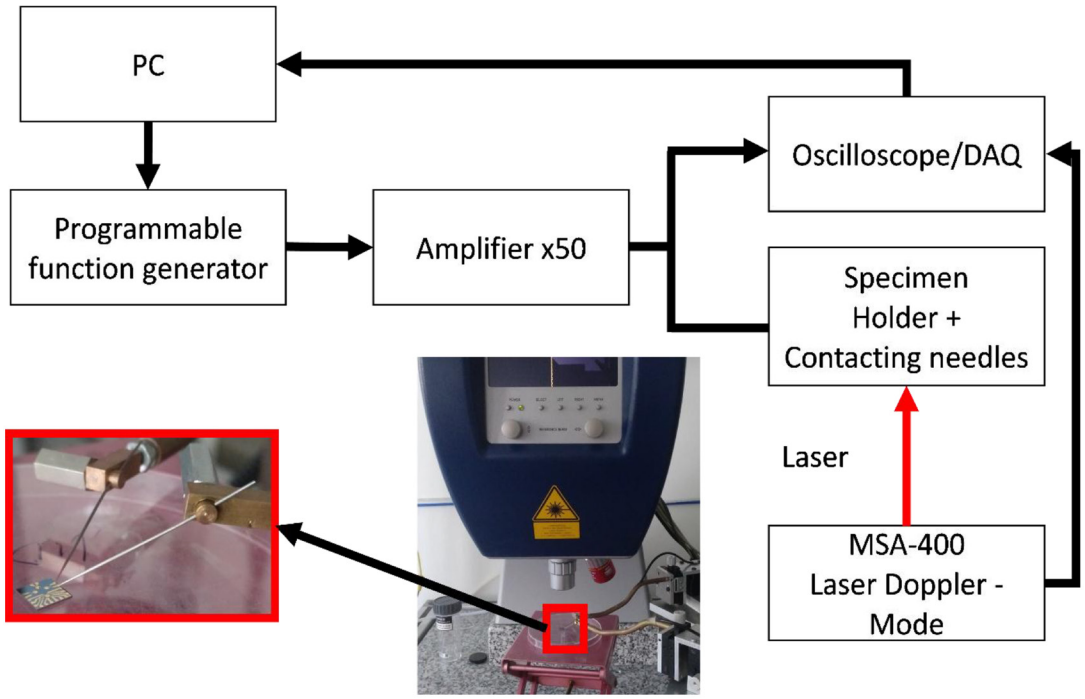

Figure 6. Schematics of the measurement setup using a POLYTEC MSA-400 to determine the velocities during the bistable switching process. The pictures show a photograph of the hardware realization including a specimen electrically contacted with prober needles.

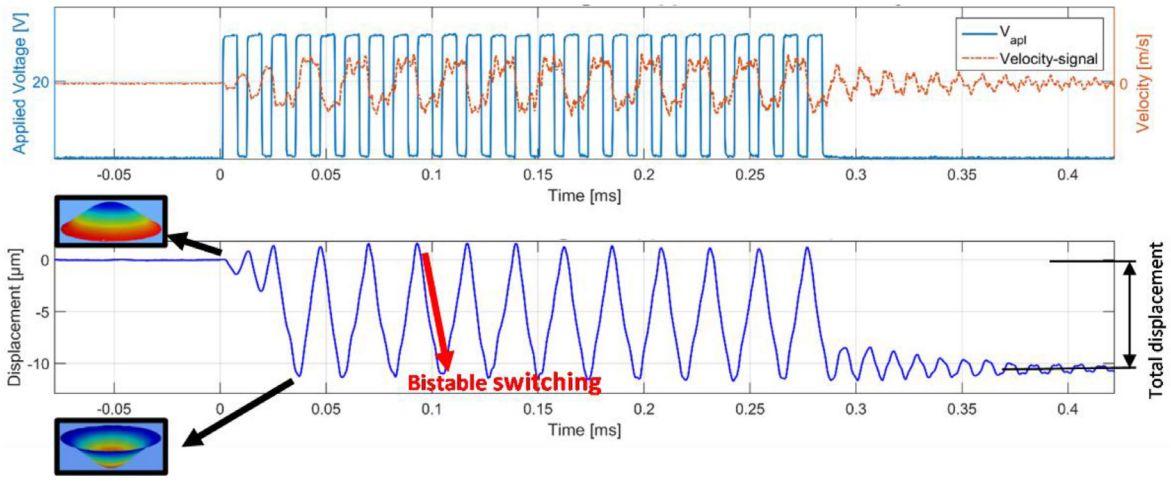

Figure 7. The top graph shows the applied signal (blue) and the measured velocity (red), whereas the bottom graph shows the calculated displacement transient during a multiple bistable switching process. This membrane with a diameter of 700 μm needs a minimum of three pulses at 79.5 kHz to switch from the upper to the lower ground state. The pictures show the two possible states of the membrane with the upper (left side) and the lower ground state (right side) and the definition of the total displacement.

a multiple of the switching frequency can stimulate a 'smooth' transition, otherwise it can interfere with the switching process. The switching frequency strongly depends on geometric parameters [25].

Figure 9 shows the results of a typical test pulse series with peak to peak voltages of 30 V and stepwise increased frequency, whereas the circle points represent the measured pulses needed to switch the ground state. Furthermore, the red line represents the measured FFT (fast Fourier transform) amplitude due to an applied white noise signal generated with the function generator due to broadband excitation and an amplitude of 0.4 V used to investigate the dependence of the actuation schemes to the fundamental resonance frequency of the membrane. An FFT of the dynamic membrane response in each ground state to a white noise excitation is performed with a sampling frequency of 1.28 MHz, a measurement time of 409.6 ms and a resolution of 2.44 Hz, which is the maximum sampling frequency of the used POLYTEC MSA-400. The dynamic response is recorded at 96 measurement points spread over the membrane and averaged prior to the FFT (figure 9, red line).

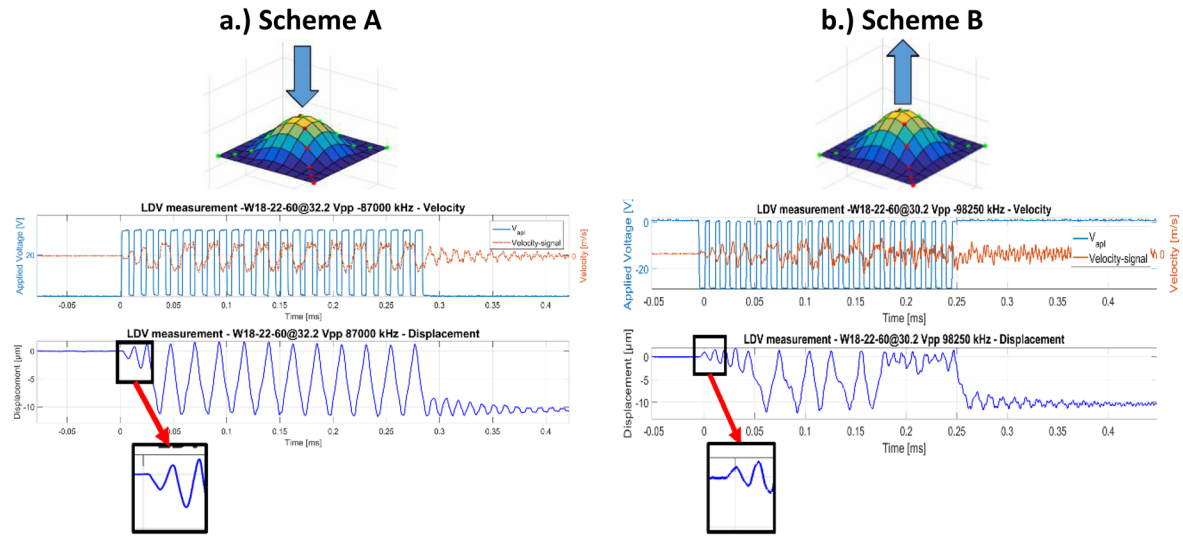

Figure 8. The two schemes where (a) shows the excitation with positive voltage pulses resulting at the onset of the periodic switching in a negative membrane displacement in the upper ground state (highlighted) and (b) the excitation with negative voltage pulses resulting in contrast in a positive displacement response. Both excitation schemes are able to switch the ground state.

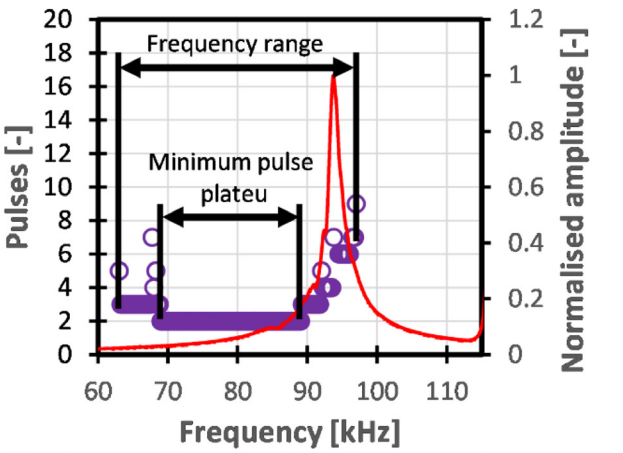

Figure 9. Measurement results of a stepwise increased frequency pulse test series, also called pulse response graph, indicating the number of pulses needed for switching (circle). As red line, the FFT amplitude (right y-axis) as response to a white noise excitation is displayed. The characteristic minimum pulse plateau as well as the used switching pulse frequency range of a bistable membrane with a diameter of 800 μm for the switching from the lower to the upper ground state are marked.

4. Experimental results

The dynamic characteristics of each ground state of the different membranes were measured with the LDV. Important parameters are the fundamental resonance frequency in both states and the total displacement during the switching process. The results are shown in table 3. The total displacement was measured from the transient between the starting point and the maximum or minimum, depending on the ground state and is illustrated in figure 7 on the bottom graph. As shown in [25], the residual stress σ_{ges} can be calculated when the material parameters (i.e. Young's modulus and Poisson's ratio), the geometric parameters (i.e. radius and thickness) and the initial deflection w_0 are known.

The dominant resonance frequency of a membrane depends on the stress, radius, thickness and density of the material [26]. When keeping the latter parameters fixed, e.g. a more compressive stress shifts the dominant resonance frequency to higher values. The measurement results from table 3 clearly show a difference in the first fundamental resonance frequency between both bistable states independent of the bistable membrane design. It is reasonable to assume, that this behaviour is a result of the membrane-related asymmetry due to the stacked structure. As expected, larger diameters show higher displacements when switching between the ground states, which is also indicated by the calculations of figure 3. Compared to the experimental results, the analytic calculations with equation (1) show an average deviation to lower values of about 16% due to assumptions such as an uniform stress distribution. The membranes were selected to have similar resonance frequencies. The results show a higher total effective to critical stress ratio σ_{ges}/σ_c in those membranes with larger diameters, which leads to higher initial deflections. This can be seen in figure 2 a by the increased separation of both minima when enhancing the σ/σ_c ratio. It is also noticeable that the membrane with a diameter of 600 μm has nearly similar fundamental resonance frequencies in both ground states at 100.1 kHz and 102.2 kHz, whereas the difference between the upper and lower state are significantly larger for membranes with diameters of 700 and 800 μm, respectively.

4.1. Evaluation of excitation schemes for switching between bistable states

In this section, we show the differences between the upper and lower ground state regarding the frequency and number of pulses required to initiate a switching process.

Figure 10 shows the result of a pulse response analysis. The first and second columns show the number of pulses required to initiate switching and the FFT when applying a white noise

Table 3. Key parameters of the membranes, whereas FRF stands for fundamental resonance frequency. The Young's modulus E and the passion ratio ν are the same for all membranes.

	Diameter [μm]	Thickness [μm]	1st FRF @ upper state [kHz]	1st FRF @ lower state [kHz]	Switching displacement—measured [μm]	Switching displacement—analytical [μm]	Impedance @ 50 kHz [kΩ]
A	600	3.13	102.2	100.1	11.2	9.7	39.2
B	700	3.13	100.1	86.2	12.4	10.3	32.65
C	800	3.13	107.7	94	13.1	11	24.5

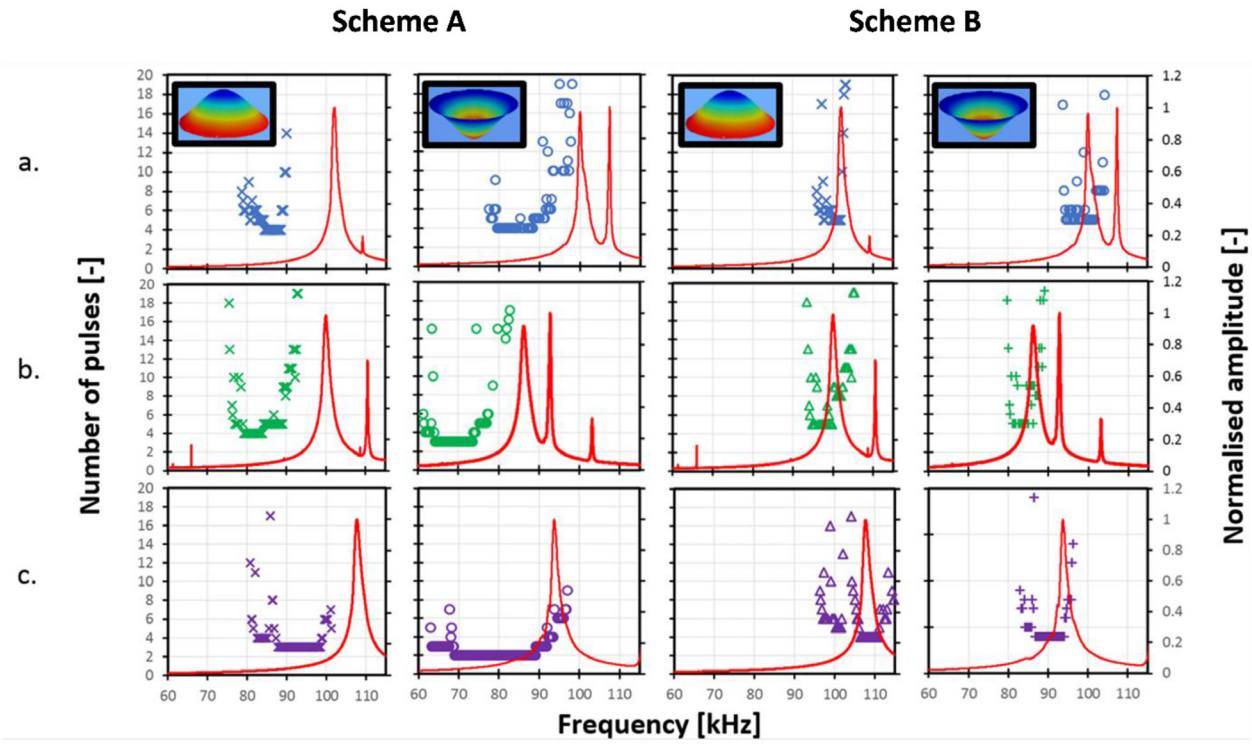

Figure 10. The graphs show the number of rectangular pulses required to initiate a switching process. The averaged FFT over the whole membrane is also shown (red). The first and second columns show the results for the upper and lower ground state using Scheme A (i.e. pulses with positive voltage) and the third and fourth columns show the results for the upper and lower ground state using Scheme B (i.e. pulses with negative voltage). The membrane diameter is varied in the different rows from (a) 600 μm (b) 700 μm to (c) 800 μm.

signal for the upper and lower ground state using scheme A. The third and fourth rows provide the same information, but for the upper and lower ground state using scheme B. Different membrane diameters are shown in rows (a)–(c) for 600, 700 and 800 μm membranes, respectively. Switching from the lower to the upper ground state always features a wider minimum pulse plateau in the range of 60–115 kHz. Nearly all of the membranes are initially in the upper ground state after the manufacturing process, which indicates that this state is preferred due to the asymmetric membrane architecture. The energy calculations in figure 2 based on equation (3) assume a uniformly distributed stress in the membrane, which is not valid due to the asymmetry introduced with the additional layers on the membrane. Again, the asymmetric membrane configuration presented in this study will result in an asymmetry in the potential energy characteristics with a shallower, local minimum for the lower compared to the upper ground state. The switching from the bottom ground state to the upper ground state was performed easier than vice versa, which is in good agreement with the analytical model (see figure 3(b)). It is assumed, that this asymmetry in both potential energy minima also directly affects the resonance frequency of the membrane, resulting in the observed variation of resonance frequency when comparing the upper and lower ground states. This is due to the narrowing and deepening of the potential energy characteristics of the upper compared to the lower state, which results in an effective stiffening of the membrane, so that a higher resonance frequency results.

Figure 10 clearly illustrates that scheme A is more effective for initiating switching between the stable states compared to scheme B. This behaviour can be explained by higher slope in the potential energy (see figure 2(b)) when the membrane gets more deflected at the start of the first pulse. Scheme A shows a larger frequency range and minimum pulse plateau width. Scheme B is most effective near the fundamental resonance peak, while for A the minimum pulse plateau is limited to frequencies below the resonance peak. The absolute minimum number of pulses required to initiate switching was measured when switching to the upper ground state with two pulses at samples having the largest membrane diameter of 800 μm. However, the potential

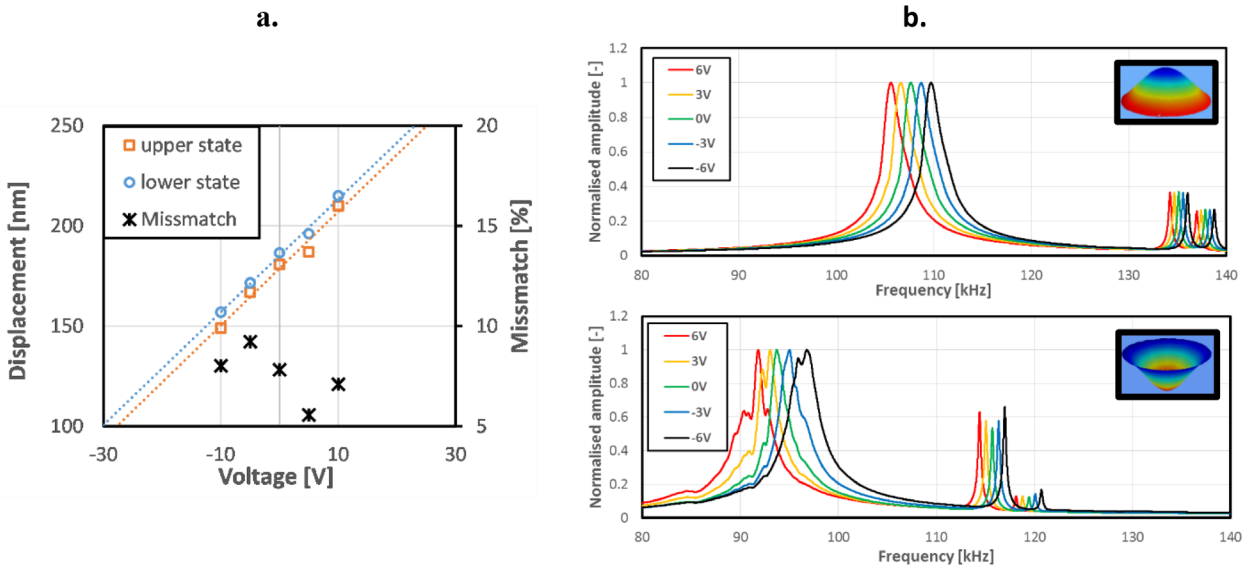

Figure 11. (a) The displacement of a membrane 800 μm in diameter when stimulated with a sine voltage (10 V_{pp} @ 20 kHz) at different DC offset values in the range of −10 to 10 V in both the upper (squares) and the lower ground state (circles) and the average mismatch of both ground states when using the stress values from table 1 and equation (4) with different voltages in equation (1). The dotted lines serves as guide to the eye. (b) The FFT spectrum of the 800 μm diameter membrane using different offset voltages. The top graph shows the results for the upper ground state and the bottom graph for the lower ground state.

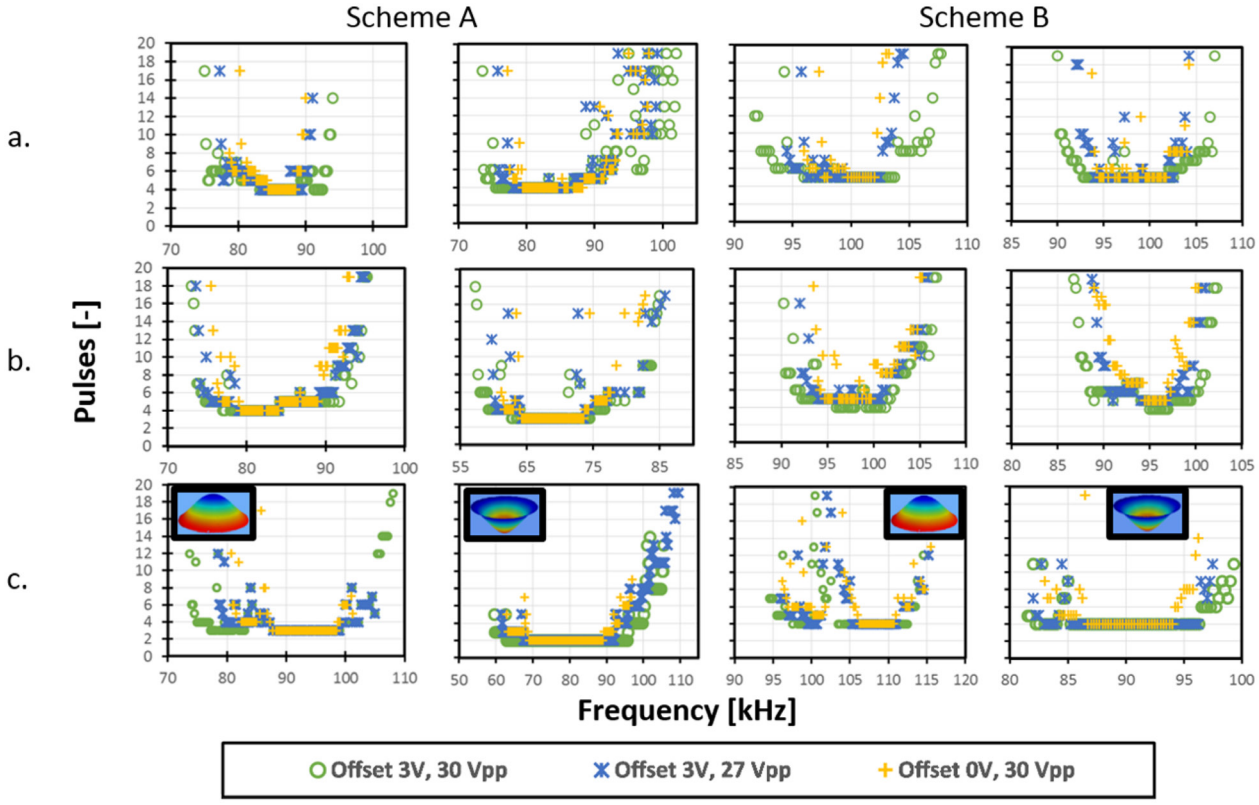

Figure 12. The measurement results for pulse response graphs with rectangular pulses using 30 V_{pp} and 3 V offset (green-circle), 27 V_{pp} and 3 V offset (blue crosses and for comparison 30 V_{pp} and no offset (yellow-cross) for (a) 600 μm, (b) 700 μm and (c) 800 μm diameter membranes. The lefts side shows the results for scheme A (positive pulses) and the right side the results for scheme B (negative pulses).

energy is in the same range and the piezoelectric active area for actuation is largest for membrane C. Therefore, the membrane can reach higher displacements and therefore switching is initiated in a wider minimum pulse plateau range.

4.2. Enlarging the minimum pulse plateau width by applying an offset

An offset can change the σ/σ_c stress ratio in the membrane and thus, influences the displacement (see equation (4)). This can be further demonstrated with a straightforward experiment by applying a sine voltage with 10 V_{pp} at 20 kHz and varying bias offsets in the range of −10 to 10 V to a membrane with 800 μm diameter. As a consequence, the dynamic displacement amplitude increases from 149 to 210 nm in the upper ground state due to the stretched potential energy characteristics around the minimum with decreasing σ/σ_c ratio (see figure 2). This is shown in figure 11 a with the displacement amplitude calculated from LDV measurements for the upper (square points) and lower ground state (circular points). The difference between the analytical model and the measured displacement values shown in figure 11(a) was calculated with equation (4) in (1), using the membrane stress values from table 1 with different voltages. E.g. when using a 10 V bias and a 10 V_{pp} excitation, the difference in the potential well minima in both stable states when applying 15 V and 5 V were evaluated. The mismatch was averaged over both bistable states and shows a good agreement with the measurements indicated by a mismatch in the range of 5.4% to 9.2%.

Also, a more compressively stressed membrane shows a higher fundamental resonance frequency. A positive voltage shifts the total effective stress of the membrane to towards a tensile value, thus resulting in a decrease of the dominant resonance frequency. This behaviour can be observed in the FFT of a 800 μm diameter membrane when applying a white noise signal with different offset bias voltages. This is illustrated in figure 11(b), where the top graph shows the results for the upper ground state and the bottom graph for the lower ground state with different offset values. A positive offset should increase the width of the minimum pulse plateau and/or decrease the required amount of rectangular pulses due to the lower σ/σ_c ratio.

The results are shown for membranes under different biasing voltages in figure 12 for (a) 600 μm, (b) 700 μm and (c) 800 μm membranes. The first and second column shows the results for scheme A with the upper and lower ground state as the initial membrane state. The third and fourth columns show the results for scheme B for both upper and lower initial state. All membranes showed a subsequently increased minimum pulse plateau width when using 30 V_{pp} and 3 V offset and 27 V_{pp} using 3 V offset, respectively, when compared to the 30 V_{pp} excitation without offset. The minimum pulse plateau of the 700 μm membrane was lowered from 5 to 4 pulses for both initial states when applying a 3 V offset and 30 V_{pp} with scheme B, as it was not the case for scheme A. The lower compressive stress in the membrane due to the applied offset expands the frequency range and the minimum pulse plateau needed to switch, independent of the excitation scheme and the ground state.

5. Conclusions

In this study, we investigated the dynamic behavior of bistable MEMS membranes with integrated piezoelectric AlN transducers prior to and during switching between both ground states. We demonstrated the different mechanical behavior of the membranes for the lower and upper ground state. This means that the resonance frequency of the lower ground state was significant reduced due to the asymmetric membrane stack. In contrast, the upper ground state is the energetically preferred state of the membrane. Two excitation schemes were introduced for initiating switching, whereas the first comprises positive and the second negative rectangular electrical pulses to the piezoelectric transducers. We found, that the minimum amount of pulses required to initiate switching is frequency dependent, thus most membranes feature a minimum plateau region below their resonance frequency. The width and height of this plateau is strongly dependent on both the radius and the ground state prior to switching. Furthermore, the minimum pulse plateau covering the widest frequency range is always in the lower ground state. In general, we found that the first excitation scheme is more effective to initiate switching featuring both a wide frequency range of the minimum pulse plateau and a smaller minimum amount of required pulses. When applying a fixed, positive bias voltage to the piezoelectric transducers the total effective compressive stress in the membranes is reduced, which manifests in lower resonance frequencies. This effect is present in all membranes for both excitation schemes. Furthermore, an increase of the bias voltage enhances the frequency range of the minimum pulse plateau for both actuation schemes while typically also reducing the minimum amount of pulses required to initiate switching. All in all, basic features and requirements are presented in this study how to switch bistable membranes from one ground state to the other with integrated piezoelectric transducers of moderate actuation potential, thus hopefully stimulating the field of low-power MEMS sensors and actuators for a large application range in the future.

Acknowledgments

This project has been supported by the COMET K1 centre ASSIC Austrian Smart Systems Integration Research Centre. The COMET—Competence Centres for Excellent Technologies- Programme is supported by BMVIT, BMWFW and the federal provinces of Carinthia and Styria. The authors acknowledge the TU Wien University Library for financial support through its Open Access Funding Programme.

ORCID iDs

M Dorfmeister https://orcid.org/0000-0002-8417-9612

References

[1] Tanaka M 2007 An industrial and applied review of new MEMS devices features *Microelectron. Eng.* **84** 1341–4

[2] Cook-Chennault K A, Thambi N and Sastry A M 2008 Powering MEMS portable devices—a review of non-regenerative and regenerative power supply systems with special emphasis on piezoelectric energy harvesting systems *Smart Mater. Struct.* **17** 043001

[3] Iannacci J 2019 Microsystem based energy harvesting (EH-MEMS): powering pervasivity of the internet of things (IoT)—a review with focus on mechanical vibrations *J. King Saud Univ.—Sci.* **31** 66–74

[4] Wang D-A, Pham H-T and Hsieh Y-H 2009 Dynamical switching of an electromagnetically driven compliant bistable mechanism *Sensors Actuators* A **149** 143–51

[5] Uusitalo J-P, Ahola V, Soederlund L, Linjama M, Juhola M and Kettunen L 2010 Novel bistable hammer valve for digital hydraulics *Int. J. Fluid Power* **11** 35–44

[6] Capanu M, Boyd J G and Hesketh P J 2000 Design, fabrication, and testing of a bistable electromagnetically actuated microvalve *J. Microelectromech. Syst.* **9** 181–9

[7] Schomburg W K and Goll C 1998 Design optimization of bistable microdiaphragm valves *Sensors Actuators* A **64** 259–64

[8] Qiu J, Lang J H and Slocum A H 2004 A curved-beam bistable mechanism *J. Microelectromech. Syst.* **13** 137–46

[9] Miao X, Dai X, Wang P, Ding G and Zhao X 2011 Design, fabrication and characterization of a bistable electromagnetic microrelay with large displacement *Microelectron. J.* **42** 992–8

[10] Andò B, Baglio S, Bulsara A R, Marletta V, Medico I and Medico S 2013 A double piezo—snap through buckling device for energy harvesting *2013 Transducers Eurosensors XXVII: The 17th Int. Conf. on Solid-State Sensors, Actuators and Microsystems (Transducers Eurosensors XXVII)* pp 43–5

[11] Timoschenko S 1959 *Theory of Plates and Shells* (New York: McGraw-Hill)

[12] Schomburg W K 2011 *Introduction to Microsystem Design* (Berlin: Springer)

[13] Qiu J, Lang J H, Slocum A H and Weber A C 2005 A bulk-micromachined bistable relay with *U*-shaped thermal actuators *J. Microelectromech. Syst.* **14** 1099–109

[14] Sun X-Q, Farmer K R and Carr W N 1998 A bistable microrelay based on two-segment multimorph cantilever actuators *Proc. MEMS 98. IEEE. Eleventh Annual International Workshop on Micro Electro Mechanical Systems. An Investigation of Micro Structures, Sensors, Actuators, Machines and Systems (Cat. No.98CH36176)* pp 154–9

[15] Qui J, Lang J H, Slocum A H and Strumpler R 2003 A high-current electrothermal bistable MEMS relay *IEEE The Sixteenth Annual Int. Conf. on Micro Electro Mechanical Systems, 2003. MEMS-03 (Kyoto)* pp 64–7

[16] Casals-Terre J, Fargas-Marques A and Shkel A M 2008 Snap-action bistable micromechanisms actuated by nonlinear resonance *J. Microelectromech. Syst.* **17** 1082–93

[17] Schneider M, Bittner A and Schmid U 2015 Improved piezoelectric constants of sputtered aluminium nitride thin films by pre-conditioning of the silicon surface *J. Phys. Appl. Phys.* **48** 405301

[18] Dorfmeister M, Kössl B, Schneider M and Schmid U 2019 A novel Bi-stable MEMS membrane concept based on a piezoelectric thin film actuator for integrated switching *MDPI Eurosens. Proc.* **2** 912

[19] Frischmuth T, Schneider M, Maurer D, Grille T and Schmid U 2016 High temperature annealing effects on the chemical and mechanical properties of inductively-coupled plasma-enhanced chemical vapor deposited a-SiC:H thin films *Thin Solid Films* **611** 6–11

[20] Takuro I 2019 *Fundamentals of Piezoelectricity* (Oxford: Oxford University Press)

[21] Stephen D 2002 *Microsystem Design* (Berlin: Springer)

[22] Schneider M, Bittner A and Schmid U 2014 Thickness dependence of Young's modulus and residual stress of sputtered aluminum nitride thin films *Appl. Phys. Lett.* **105** 201912

[23] Wright A F 1997 Elastic properties of zinc-blende and wurtzite AlN, GaN, and InN *J. Appl. Phys.* **82** 2833–9

[24] Casset F 2011 Piezoelectric membrane actuator design *12th Int. Conf. on Thermal, Mechanical Multi-Physics Simulation and Experiments in Microelectronics and Microsystems* pp 1/5–5/5

[25] Dorfmeister M, Schneider M and Schmid U 2018 Static and dynamic performance of bistable MEMS membranes *Sensors Actuators* A **282** 259–68

[26] Schmid S 2015 Organic resonant MEMS devices *Resonant MEMS* (New York: Wiley) pp 233–60